First-order P-wave ray synthetic seismograms in inhomogeneous, weakly anisotropic, layered media

Ivan Pšenčík [1] and Véronique Farra [2],

[1]Institute of Geophysics, Acad. Sci. of Czech Republic, Boční II, 141 31 Praha 4, Czech Republic. E-mail: ip@ig.cas.cz
[2]Institut de Physique du Globe de Paris, Sorbonne Paris Cité, Université Paris Diderot, UMR 7154 CNRS, F-75005 Paris, France. E-mail: farra@ipgp.fr

SUMMARY

The first-order ray tracing (FORT) and dynamic ray tracing (FODRT) for P waves propagating in inhomogeneous, weakly anisotropic media are extended from smooth to layered media. All the basic formulae necessary for the transformation of FORT and FODRT quantities at the points of reflection/transmission are given. Accuracy of results is tested by comparison of approximate results with results obtained from a standard ray tracer.

Keywords: inhomogeneous layered media, perturbation methods, P waves, seismic anisotropy, seismic ray theory, synthetic seismograms.

1 INTRODUCTION

First-order ray tracing (FORT) and dynamic ray tracing (FODRT) for P waves (Pšenčík and Farra, 2005, 2007) provide approximate, but simple and quite accurate, way of computing traveltimes and geometrical spreading of seismic waves propagating in inhomogeneous, weakly, and even moderately, anisotropic media. FORT and FODRT are procedures based on the perturbation theory, in which deviations of anisotropy from isotropy are considered to be small perturbations. The basic idea of FORT and FODRT is to replace the exact eigenvalue and corresponding eigenvector of the Christoffel matrix related to the studied wave (in our case P wave) by their first-order counterparts.

In this paper, we are extending the applicability of P-wave FORT and FODRT to layered media. Basic steps in this extension are the introduction of a rule (Snell's law) for the determination of first-order slowness vectors of reflected and transmitted P waves into FORT and the transformation of FODRT quantities across interfaces. For the transformation of the first-order slowness vectors across interfaces, we use the algorithm described

Seismic Waves in Complex 3-D Structures, Report 23, Charles University, Faculty of Mathematics and Physics, Department of Geophysics, Praha 2013, pp. 185–202

by Dehghan et al. (2007) or Farra and Pšenčík (2010). For the transformation of FODRT quantities across interfaces, we use equations formally identical to the exact ones derived by Farra and Le Bégat (1995), with exact quantities replaced by their first-order counterparts. Another difference with respect to standard approaches appears in the transformation of the first-order ray amplitudes across interfaces. After reflection/transmission, instead of dealing with a P and two separate S waves, we deal with a P and a single, coupled S wave, Farra and Pšenčík (2010). This makes our approach similar to the approaches used in isotropic media.

In Section 2, we introduce the first-order P-wave ray theory Green's function for layered, inhomogeneous, weakly anisotropic media. In Section 3, we review the basics of FORT and FODRT in smooth media. Section 4 contains the review of the transformation rules of the slowness vectors across an interface between two inhomogeneous, weakly anisotropic media. In Section 5, we present formulae for the transformation of the dynamic ray tracing quantities across an interface. Section 6 contains a brief description of the determination of the first-order ray amplitudes of waves generated by the incidence of the first-order P wave at an interface. Section 7 contains the main contribution of this paper, the tests of the accuracy of the formulae given in the preceding sections. The approximately computed results are compared with corresponding exact results obtained by standard ray theory (Červený, 2001), specifically by the results of the program package ANRAY (Gajewski and Pšenčík, 1990). Section 8 contains concluding remarks.

The lower-case indices $i, j, ...$ take the values of 1,2,3, the upper-case indices $I, J, ...$ take the values of 1,2. The Einstein summation convention over repeated indices is used. The superscript G stands for R in case of a reflected and for T in case of a transmitted wave.

2 FIRST-ORDER P-WAVE GREEN's FUNCTION

The first-order P-wave ray theory Green's function $G_{in}(R, S, \omega)$ along a first-order P-wave ray from source S to receiver R situated in a layered, inhomogeneous, weakly anisotropic medium represents a simple generalization of the Green's function for smooth media, see Pšenčík and Farra (2007; eq.(9)). In layered media, it has the form:

$$G_{in}(R,S,\omega) = \frac{f_n^{[3]}(S) f_i^{[3]}(R) \exp[iT^C(R,S) + i\omega\tau(R,S)]}{4\pi[\rho(S)\rho(R)c(S)c(R)]^{\frac{1}{2}}\mathcal{L}(R,S)} \times \Pi_{k=1}^{K} \frac{\mathcal{C}(O_k^G)}{\mathcal{C}(O_k)} \left[\frac{\rho(O_k^G)c(O_k^G)\cos i(O_k^G)}{\rho(O_k)c(O_k)\cos i(O_k)}\right]^{\frac{1}{2}} . \quad (1)$$

The Green's function (1) is calculated along a first-order ray and most of quantities, on which it depends, are of the first order. They are all defined in the following sections. Symbol $f_i^{[3]}$ in equation (1) represents i-th component of the first-order P-wave polarization vector $\mathbf{f}^{[3]}$, symbols c and ρ denote the first-order phase velocity and the density, respectively. For the first-order relative geometrical spreading we use the symbol $\mathcal{L}$. Symbol $\tau(R, S)$ denotes the traveltime from source S ($\tau = \tau_0$) to receiver R. In all following

considerations, we consider its second-order approximation, $\tau = \tau^{\{2\}}$. Symbol $T^C(R,S)$ in equation (1) represents the complete phase shift due to caustics along the first-order ray. The k-th point of incidence and of reflection/transmission at an interface is denoted O_k and O_k^G, respectively. Of course, the two points coincide. Symbols $\mathcal{C}(O_k)$ and $\mathcal{C}(O_k^G)$ denote the first-order scalar P-wave spreading-free amplitude factors of incident and generated waves, respectively. Finally, symbols $i(O_k)$ and $i(O_k^G)$ are reserved for angles of incidence and reflection/transmission, respectively. They are defined as acute angles made by the corresponding slowness vectors and normal $\mathbf{N}$ to the interface.

For the evaluation of the quantities appearing in equation (1), we have to perform FORT and FODRT. The necessary equations are given in the following section.

3 TRAVEL TIME AND SPREADING IN SMOOTH MEDIA

The first-order P-wave ray in an inhomogeneous, weakly anisotropic medium can be obtained by solving FORT equations:

$$\frac{dx_i}{d\tau} = \frac{1}{2}\frac{\partial G^{[3]}(x_m,p_m)}{\partial p_i}, \qquad \frac{dp_i}{d\tau} = -\frac{1}{2}\frac{\partial G^{[3]}(x_m,p_m)}{\partial x_i}. \tag{2}$$

Here x_i and p_i are the Cartesian coordinates of the first-order P-wave ray and the components of the corresponding first-order slowness vectors $\mathbf{p}$, respectively. Parameter τ is the first-order traveltime calculated along the first-order ray. Symbol $G^{[3]}$ denotes the first-order P-wave eigenvalue (greatest) of the generalized Christoffel matrix with elements Γ_{ik}:

$$\Gamma_{ik}(x_m,p_m) = a_{ijkl}(x_m)p_j p_l \ . \tag{3}$$

The fourth-order tensor a_{ijkl} is the tensor of density-normalized elastic moduli, $a_{ijkl} = c_{ijkl}/\rho$, c_{ijkl} being elements of the fourth-order tensor of elastic moduli, ρ is the density.

The initial conditions for the ray-tracing equations (2) for $\tau = \tau_0$ read:

$$x_i(\tau_0) = x_i^0, \qquad p_i(\tau_0) = p_i^0. \tag{4}$$

Here, x_i^0 are the coordinates of source point $\mathbf{x}^0$, and $p_i^0 = n_i^0/c_0$ are the components of the first-order slowness vector $\mathbf{p}^0$ at the source. Symbol c_0 denotes the first-order approximation of P-wave phase velocity in the direction $\mathbf{n}^0$ at source point $\mathbf{x}^0$. The vector $\mathbf{n}^0$ is specified by two ray parameters γ_I: for example, take-off angles $\gamma_1 = \phi_0$ and $\gamma_2 = \delta_0$. Then:

$$n_1^0 = \cos\phi_0 \cos\delta_0, \quad n_2^0 = \sin\phi_0 \cos\delta_0, \quad n_3^0 = \sin\delta_0 \ . \tag{5}$$

FORT equations (2) provide directly first-order traveltimes. Traveltimes of second-order accuracy can be simply computed by quadratures along first-order rays (Pšenčík and Farra, 2005). The second-order traveltime formula reads:

$$\tau^{\{2\}}(\tau,\tau_0) = \tau + \Delta\tau(\tau,\tau_0) \ . \tag{6}$$

Here τ denotes the first-order traveltime obtained by integrating the ray tracing system (2). Symbol $\Delta\tau$ denotes the second-order traveltime correction obtained by quadratures along the first-order ray:

$$\Delta\tau = -\frac{1}{2}\int_{\tau_0}^{\tau} \frac{B_{13}^2(\tau) + B_{23}^2(\tau)}{1 - \frac{1}{2}[B_{11}(\tau) + B_{22}(\tau)]} d\tau. \tag{7}$$

The elements of symmetric matrix $\mathbf{B}(\tau)$ are given by the formula

$$B_{jl}(\tau) = \Gamma_{ik}(x_m, p_m) e_i^{[j]} e_k^{[l]}, \tag{8}$$

where $x_m = x_m(\tau)$ and $p_m = p_m(\tau)$. Symbols $e_i^{[j]} = e_i^{[j]}(\tau)$ in (8) denote the components of vectors $\mathbf{e}^{[j]}$ forming an orthonormal triplet. Vectors $\mathbf{e}^{[1]}$ and $\mathbf{e}^{[2]}$ are perpendicular to the vector $\mathbf{e}^{[3]}$ chosen so that $\mathbf{e}^{[3]} = c\mathbf{p}$. Here c is the first-order phase velocity and $\mathbf{p}$ the first-order slowness vector. At any point of the first-order P-wave ray, vector $\mathbf{e}^{[3]}$ can be determined from the solution of the second set of FORT equations (2). Vectors $\mathbf{e}^{[K]}$ can be chosen arbitrarily in the plane perpendicular to $\mathbf{p}$. Elements of the matrix $\mathbf{B}$ are, in fact, projections of elements of the generalized Christoffel matrix into the vectors $\mathbf{e}^{[j]}$. The element B_{33} corresponding to P wave is unit, $B_{33} = 1$, along the first-order ray.

The P-wave first-order dynamic ray tracing in an inhomogeneous, weakly anisotropic medium is a system of linear differential equations:

$$\begin{aligned}
\frac{dX_i^{(J)}}{d\tau} &= \frac{1}{2}\Big(\frac{\partial^2 G^{[3]}(x_m, p_m)}{\partial p_i \partial x_j} X_j^{(J)} + \frac{\partial^2 G^{[3]}(x_m, p_m)}{\partial p_i \partial p_j} Y_j^{(J)}\Big) \ , \\
\frac{dY_i^{(J)}}{d\tau} &= -\frac{1}{2}\Big(\frac{\partial^2 G^{[3]}(x_m, p_m)}{\partial x_i \partial x_j} X_j^{(J)} + \frac{\partial^2 G^{[3]}(x_m, p_m)}{\partial x_i \partial p_j} Y_j^{(J)}\Big) \ .
\end{aligned} \tag{9}$$

The quantities $X_i^{(J)} = \partial x_i/\partial\gamma_J$ and $Y_i^{(J)} = \partial p_i/\partial\gamma_J$ describe variations along the wavefront of the coordinates x_i and of the components p_i of the first-order slowness vector due to the variations of the ray parameters γ_I. The system (9) is obtained by the differentiation of the FORT equations (2) with respect to γ_J. If we choose the ray parameters γ_I as the take-off angles ϕ_0 and δ_0, see eq.(5), the initial conditions for the FODRT, corresponding to (4) have the form:

$$X_i^{(J)}(\tau_0) = 0, \quad Y_i^{(J)}(\tau_0) = c_0^{-1}(Z_{iJ} - p_i^0 v_k^0 Z_{kJ}) \ , \tag{10}$$

where

$$\begin{aligned}
Z_{11} = -\sin\phi_0\cos\delta_0, \quad Z_{21} = \cos\phi_0\cos\delta_0, \quad Z_{31} = 0 \ , \\
Z_{12} = -\cos\phi_0\sin\delta_0, \quad Z_{22} = -\sin\phi_0\sin\delta_0, \quad Z_{32} = \cos\delta_0 \ .
\end{aligned} \tag{11}$$

In eqs (10), c_0 is again the first-order phase velocity at the point $\mathbf{x}^0$, v_i^0 is the i-th component of the first-order ray-velocity vector, $\mathbf{v}^0 = d\mathbf{x}/d\tau$, at $\mathbf{x}^0$. It can be obtained from the first set of ray tracing equations (2). The results of FODRT can be used for many purposes, among them, for example, for the computation of the first-order relative geometrical spreading $\mathcal{L}(\tau)$:

$$\mathcal{L}(\tau) = |\mathbf{X}^{(1)} \times \mathbf{X}^{(2)}|^{1/2} \tag{12}$$

along the first-order ray.

Finally, we present formula for the first-order P-wave polarization vector $\mathbf{f}^{[3]}$ used in (1). It reads:

$$\mathbf{f}^{[3]}(\tau) = \frac{B_{13}(\tau)\mathbf{e}^{[1]}(\tau) + B_{23}(\tau)\mathbf{e}^{[2]}(\tau)}{1 - \frac{1}{2}[B_{11}(\tau) + B_{22}(\tau)]} + \mathbf{e}^{[3]}(\tau) \ . \tag{13}$$

Here $B_{ij}(\tau)$ are the elements of the matrix $\mathbf{B}(\tau)$, given in equation (8), and $\mathbf{e}^{[i]}$ are the vectors of the orthonormal vectorial basis described after equation (8). Note that vector $\mathbf{e}^{[3]}$ also represents the zero-order P-wave polarization vector.

When transforming the first-order ray amplitudes across an interface, we shall also need vectors $\mathbf{f}^{[1]}$ and $\mathbf{f}^{[2]}$, which define the first-order polarization plane of generated coupled S waves at the point of incidence. At the point of incidence, they are defined as

$$\mathbf{f}^{[K]} = \mathbf{e}^{[K]} + \frac{B_{K3}}{1 - B_{33}}\mathbf{e}^{[3]} \ . \tag{14}$$

Please note an important difference between equations (13) and (14). The orthonormal basis $\mathbf{e}^{[i]}$ in (13) is constructed along the first-order P-wave ray. Vector $\mathbf{e}^{[3]}$ is parallel to the first-order P-wave slowness vector $\mathbf{p}$. The orthornormal basis $\mathbf{e}^{[i]}$ in (14) is constructed only at the point of reflection/transmission, and it is related to a generated coupled S wave. In this case, vector $\mathbf{e}^{[3]}$ is parallel to slowness vector $\mathbf{p}$ of the generated coupled S wave. The elements of matrix $\mathbf{B}(\tau)$ in (14) are also calculated in the orthonormal basis related to the coupled S wave.

4 TRANSFORMATION OF FORT AT AN INTERFACE

Let us consider a generally curved interface $\Sigma(x_m) = 0$ and a P wave incident at it. The slowness vector $\mathbf{p}^G$ of a generated reflected or transmitted P or coupled S wave at the point of incidence of a P-wave ray at Σ can be written in the form (Farra and Pšenčík, 2010):

$$p_i^G = b_i + \xi^G N_i = p_i - (p_k N_k)N_i + \xi^G N_i \ . \tag{15}$$

In case of the generated P wave, $\mathbf{p}^G$ corresponds to the first-order reflected/transmitted P-wave ray at the point of incidence. In case of generated coupled S wave, $\mathbf{p}^G$ corresponds to the first-order reflected/transmitted common S-wave ray at the point of incidence. The symbol $\mathbf{N}$ in (15) denotes the unit normal to interface Σ at the point of the incidence of the first-order P-wave ray at Σ,

$$N_i = \Sigma_{,i}/(\Sigma_{,k}\Sigma_{,k}) \ . \tag{16}$$

The symbol ξ^G represents the projection of $\mathbf{p}^G$ to $\mathbf{N}$:

$$\xi^G = \mathbf{p}^G \cdot \mathbf{N} \ . \tag{17}$$

Vector $\mathbf{b}$ represents the vectorial component of $\mathbf{p}^G$, tangential to Σ. It is the same for incident and all generated waves (this is an alternative expression of Snell's law), and it

is thus a known quantity. Quantity ξ^G is to be determined. It can be determined from the first-order eikonal equation, which the generated wave must satisfy at the point of incidence on the corresponding side of the interface:

$$G(b_k + \xi^G N_k) = 1 \ . \tag{18}$$

To solve equation (18), we can use an iterative procedure proposed by Dehghan et al. (2007), and described in detail by Farra and Pšenčík (2010). In it, we seek the first-order slowness vector $\mathbf{p}^G$ of a selected generated wave at the point of incidence iteratively. The j-th iteration has the form

$$p_k^{\{j\}G} = b_k + \xi^{\{j\}G} N_k \ , \tag{19}$$

where

$$\xi^{\{j\}G} = \xi^{\{j-1\}G} - \frac{G(p_m^{\{j-1\}G}) - 1}{N_k \partial G / \partial p_k (p_m^{\{j-1\}G})} \ . \tag{20}$$

The initial value $\xi^{\{0\}G}$ of the quantity $\xi^{\{j\}G}$ is determined for a reference isotropic medium. The explicit expressions for G and $\partial G/\partial p_k$ can be found in papers dealing with FORT, see more details in Farra and Pšenčík (2010).

5 TRANSFORMATION OF FODRT AT AN INTERFACE

Here we present formulae for the transformation of the first-order quantities $X_j^{(I)}$ and $Y_j^{(I)}$, calculated by FODRT in equations (9), at an interface. The transformation formulae were derived by Farra and Le Bégat (1995), the only difference here is that instead of the exact quantities, we use their first-order counterparts in the following equations. If we keep the symbols $X_j^{(I)}$ and $Y_j^{(I)}$ for the incident P wave and denote by $X_j^{(I)G}$ and $Y_j^{(I)G}$ the quantities corresponding to the reflected/transmitted P wave (the applicability of the following formulae is broader; they can also be used when a coupled S wave is the incident or generated wave), the transformation formulae read:

$$X_i^{(J)G} = P_{ik} X_k^{(J)} \ , \qquad Y_i^{(J)G} = R_{ik} X_k^{(J)} + S_{ik} Y_k^{(J)} \ . \tag{21}$$

The elements of 3×3 matrices $\mathbf{P}$, $\mathbf{R}$ and $\mathbf{S}$ have the following form:

$$P_{ij} = \delta_{ij} + \eta^{-1}(X_i^{(3)G} - X_i^{(3)}) N_j \ ,$$

$$\begin{aligned} R_{ij} = {} & \eta^{-1}(Y_i^{(3)G} - Y_i^{(3)}) N_j + (\eta^G)^{-1}(Y_j^{(3)G} - Y_j^{(3)}) N_i \\ & + (\eta\eta^G)^{-1}(X_k^{(3)G} Y_k^{(3)} - X_l^{(3)} Y_l^{(3)G}) N_i N_j \\ & + (\Sigma_{,m}\Sigma_{,m})^{-1/2}(\xi^G - \xi)\Sigma_{,lk}(\delta_{il} - (\eta^G)^{-1} X_l^{(3)G} N_i)(\delta_{kj} - \eta^{-1} X_k^{(3)} N_j) \ , \end{aligned}$$

$$S_{ij} = \delta_{ij} - (\eta^G)^{-1}(X_j^{(3)G} - X_j^{(3)}) N_i \ . \tag{22}$$

In equation (22), the quantities $X_i^{(3)}$ and $Y_i^{(3)}$ are defined as follows:

$$X_i^{(3)} = dx_i/d\tau \ , \qquad Y_i^{(3)} = dp_i/d\tau \ . \tag{23}$$

We can see that $X_i^{(3)}$ and $Y_i^{(3)}$ can be determined from equations (2) at the point of incidence. Similarly, $X_i^{(3)G}$ and $Y_i^{(3)G}$ can be determined from (2) at the same point, but with parameters corresponding to the considered generated wave and the medium, in which the wave propagates. The quantity ξ^G in (22) is given by (17), ξ is its counterpart corresponding to the incident wave, $\xi = \mathbf{p}\cdot\mathbf{N}$. Finally, η and η^G in (22) denote projections of $X_i^{(3)}$ and $X_i^{(3)G}$ into normal $\mathbf{N}$ to interface Σ, respectively:

$$\eta = X_m^{(3)} N_m \ , \qquad \eta^G = X_m^{(3)G} N_m \ . \tag{24}$$

Let us emphasize that all the above quantities are of the first order.

6 TRANSFORMATION OF FIRST-ORDER RAY AMPLITUDES AT AN INTERFACE

The first-order ray amplitudes of waves generated by the incidence at the interface Σ of the P wave propagating along the first-order ray are calculated from formally the same system of six algebraic equations as in the exact case. Compare formulae given in Gajewski and Pšenčík (1987) with Farra and Pšenčík (2010). The difference consists in the use of the first-order approximations of the slowness and polarization vectors instead of their exact values. The system of equations for the first-order amplitudes of reflected and transmitted P and coupled S waves has the form:

$$\mathcal{A}^R f_i^{[1]R} + \mathcal{B}^R f_i^{[2]R} + \mathcal{C}^R f_i^{[3]R} - \mathcal{A}^T f_i^{[1]T} - \mathcal{B}^T f_i^{[2]T} - \mathcal{C}^T f_i^{[3]T} = -\mathcal{C} f_i^{[3]} \ ,$$

$$\mathcal{A}^R T_i^{[1]R} + \mathcal{B}^R T_i^{[2]R} + \mathcal{C}^R T_i^{[3]R} - \mathcal{A}^T T_i^{[1]T} - \mathcal{B}^T T_i^{[2]T} - \mathcal{C}^T T_i^{[3]T} = -\mathcal{C} T_i \ , \tag{25}$$

where

$$T_i = \rho^{(1)} a_{ijkl}^{(1)} N_j f_k^{[3]} p_l \ ,$$

$$T_i^{[3]R} = \rho^{(1)} a_{ijkl}^{(1)} N_j f_k^{[3]R} p_l^{[3]R} \ , \quad T_i^{[3]T} = \rho^{(2)} a_{ijkl}^{(2)} N_j f_k^{[3]T} p_l^{[3]T} \ ,$$

$$T_i^{[N]R} = \rho^{(1)} a_{ijkl}^{(1)} N_j f_k^{[N]R} p_l^{[\mathcal{M}]R} \ , \quad T_i^{[N]T} = \rho^{(2)} a_{ijkl}^{(2)} N_j f_k^{[N]T} p_l^{[\mathcal{M}]T} \ . \tag{26}$$

The symbol $\mathcal{C}$ is the first-order scalar P-wave spreading-free amplitude factor, $\mathcal{C}(S) = 1$. $\mathcal{A}$ and $\mathcal{B}$ are the first-order scalar S-wave spreading-free amplitude factors. Quantities without upper indices correspond to the incident P wave, the factors with indices R and T correspond to reflected and transmitted waves. Quantities with the index [3] correspond to P waves, quantities with indices [1] and [2] correspond to the coupled S wave. Slowness vectors of generated waves are determined by the procedure described in Section 4. Vectors $\mathbf{f}^{[i]G}$ are determined from eqs (13) in case of P waves ($i = 3$) or (14) in case of coupled S waves ($i = 1, 2$).

7 TESTS OF ACCURACY

It was shown by Pšenčík and Farra (2005) that even for a model with P-wave anisotropy of about 20% $[2(c_{max}-c_{min})/(c_{max}+c_{min})\times 100\%]$, the relative error of the P-wave FORT traveltimes was less than 1%. In case of spreading (Pšenčík and Farra, 2007), the errors were larger. They could reach even 20%, although in a limited region only. This picture is similar also in layered media. In the following, we present results for two models containing an interface. One is the model consisting of a transversely isotropic layer with horizontal axis of symmetry (HTI) overlying an HTI halfspace. The anisotropy of this model is about 8%. We call the model "HTI/HTI". The other model is composed of an orthorhombic layer overlying an orthorhombic halfspace. This time, the anisotropy is about 20%. We call the model "ORT/ORT". Both models are derived from the corresponding smooth models used by Pšenčík and Farra (2005, 2007). We test the accuracy of the FORT approach by comparing FORT results for the subcritical P-wave incidence with results obtained by ANRAY package (Gajewski and Pšenčík, 1990) based on the standard ray theory.

We consider Cartesian coordinate system (x, y, z) with vertical z-axis positive downwards. The tests are performed for the VSP configuration with the source and the borehole situated in the vertical plane (x, z). The borehole is parallel to the z-axis, the vertical single-force source is at $z = 0$ km, at a distance of 1 km from the borehole. The source-time function is a windowed symmetric Gabor wavelet $\exp[-(2\pi f/\gamma)^2 t^2]cos2\pi ft$ with the dominant frequency $f = 50\ Hz$ and $\gamma = 4$. There are 33 receivers in the borehole, starting at the depth of 0.06 km, distributed uniformly with the step of 0.06 km. The deepest receiver is thus situated at the depth of 1.98 km. The three-component receivers record the vertical (positive downwards), radial (along the line source - top of the borehole; positive away from the source), and transverse components of the wave field. The recording system (RTZ) is right-handed. The radial and vertical component seismograms are shown with no differential scaling between components and traces, so true relative amplitudes can be seen. The transverse component seismograms are rather weak and, therefore, they are amplified.

For simplicity, we consider models with only vertical variation of parameters of the medium and flat horizontal interfaces. FORT and FODRT can, however, be applied to arbitrary laterally varying weakly anisotropic media with smoothly curved interfaces.

At any point of the model, parameters of the medium are determined by vertical linear interpolation of density-normalized elastic moduli $A_{\beta\gamma}$ $(\beta, \gamma = 1, 2, ..., 6)$ in the Voigt notation from values given at two horizontal levels. The moduli are specified in $(\mathrm{km/s})^2$. In both models, the density, specified in g cm^{-3}, is determined from the relation $\rho = 1.7 + 0.2\sqrt{A_{11}}$.

In the following, we test the accuracy of FORT and FODRT, not only by comparing the approximate and exact ray synthetic seismograms, but also by presenting relative errors of the second-order approximation of travel time:

$$\frac{\tau_{FORT} - \tau_{EXACT}}{\tau_{EXACT}} \times 100\% \tag{27}$$

and relative errors of the first-order geometrical spreading:

$$\frac{\mathcal{L}_{FORT} - \mathcal{L}_{EXACT}}{\mathcal{L}_{EXACT}} \times 100\% \ . \tag{28}$$

The symbol τ_{FORT} denotes the second-order travel time, which can be obtained from equations (6) and (7). The symbol $\mathcal{L}_{FORT}$ denotes the first-order geometrical spreading, which can be obtained from equation (12). The exact travel time τ_{EXACT} and the geometrical spreading $\mathcal{L}_{EXACT}$ are calculated using the ANRAY package.

7.1 HTI/HTI model

This model consists of the transversely isotropic layer separated at the depth of 1 km by the flat horizontal interface from the underlying transversely isotropic halfspace. The axis of symmetry is horizontal (HTI medium) in the layer as well as the halfspace. The anisotropy in the whole model is around 8%. In the layer, the matrices of the density-normalized elastic moduli are:

$$\begin{pmatrix} 15.71 & 5.05 & 4.46 & 0.00 & 0.00 & 0.00 \\ & 15.71 & 4.46 & 0.00 & 0.00 & 0.00 \\ & & 13.39 & 0.00 & 0.00 & 0.00 \\ & & & 4.98 & 0.00 & 0.00 \\ & & & & 4.98 & 0.00 \\ & & & & & 5.33 \end{pmatrix} \tag{29}$$

at $z = 0$ km, and

$$\begin{pmatrix} 22.25 & 7.15 & 6.32 & 0.00 & 0.00 & 0.00 \\ & 22.25 & 6.32 & 0.00 & 0.00 & 0.00 \\ & & 18.97 & 0.00 & 0.00 & 0.00 \\ & & & 7.06 & 0.00 & 0.00 \\ & & & & 7.06 & 0.00 \\ & & & & & 7.55 \end{pmatrix} \tag{30}$$

at $z = 1$ km, i.e., at the interface. In the horizontal plane $z = 0$ km, the axis of symmetry is rotated so that it is horizontal and deviates by 45^o from the x-axis (the medium is thus HTI). At $z = 1$ km, the axis of symmetry is rotated so that it is parallel to the x-axis. As the depth varies between 0 and 1 km, the axis of symmetry thus smoothly rotates, remaining horizontal. In the halfspace, the matrix of density-normalized elastic moduli is:

$$\begin{pmatrix} 35.3475 & 11.3625 & 10.0350 & 0.0000 & 0.0000 & 0.0000 \\ & 35.3475 & 10.0350 & 0.0000 & 0.0000 & 0.0000 \\ & & 30.1275 & 0.0000 & 0.0000 & 0.0000 \\ & & & 11.2050 & 0.0000 & 0.0000 \\ & & & & 11.2050 & 0.0000 \\ & & & & & 11.9925 \end{pmatrix} \ . \tag{31}$$

The elements of matrix (31) remain the same throughout the halfspace. The axis of symmetry is again rotated so that it is horizontal. At $z = 1$ km, it is parallel to the x-axis, and in the horizontal plane $z = 3$ km, it deviates by 45^0 from the x-axis. In between, as the depth varies, the axis of symmetry smoothly rotates, remaining horizontal.

In the bottom part of Figure 1, we show the diagram of first-order rays of direct (above the interface) and transmitted wave (below the interface). We can clearly see the position of the interface indicated by the points, at which rays break and transmit to the halfspace. Effect of the interface is also weakly observable on the second-order travel time curve in the upper part of Figure 1. Although the velocity contrast (the absolute value of the difference of velocities on both sides of the interface divided by their average $\times$ 100%) is not large, it is about 23%, we can observe sudden decrease in the growth of travel times with depth. We show neither exact ray diagram nor travel time curve because they perfectly coincide with the plots in Figure 1. Instead of this comparison we show relative errors of travel times and of the geometrical spreading in Figure 2.

In Figure 2 we can see the relative errors of the second-order travel time (top) and of the first-order spreading (bottom). The blue crosses correspond to the reflected wave (between depths of 0 and 1 km) and the red crosses to the transmitted wave (between depths of 1 and 2 km). We can see that traveltime errors do not exceed 0.02%, spreading errors are less than 0.5%. Chaotic behaviour of travel time errors at shallow receivers is due to inaccuracies of the two-point ray tracing procedure used for both FORT and exact computations. The spreading errors of the reflected wave increase from values of about 0.2% to over 0.4% with increasing depth. The errors of the transmitted wave are relatively small immediately below the interface, then they increase with the depth, and then decrease again after reaching the maximum of about 0.4%. We can see that the relative errors of travel time and spreading are comparable with the corresponding relative errors observed in smooth media (Pšenčík and Farra, 2007).

The above-discussed second-order travel times and first-order spreading are used in the construction of ray synthetic seismograms shown in Figure 3. Figure 3 shows exact (black) ray synthetic seismograms generated by the package ANRAY, overlayed by the approximate ray synthetic seismograms (red) calculated using FORT and FODRT procedures. We can observe the direct wave (the first arrivals between 0 and 1 km), the reflected wave (second arrivals between 0 and 1 km) and transmitted wave (arrivals between 1 and 2 km). Because the axis of symmetry of the HTI medium at the surface deviates by 45^0 from the x-axis, the direct wave in the layer has also a weak transverse component. Note that it is so weak that it had to be amplified 25 times with respect to the vertical and radial components. The transverse component of the transmitted wave is even weaker. It is because the energy of the transmitted wave is weakened by the transmission and immediately below the interface, it propagates effectively in the plane of symmetry of the TI medium in the halfspace. The reflected wave is considerably weaker than the direct wave and has nearly zero transverse component. It is because the reflections are subcritical, the velocity contrast is relatively weak and the reflection coefficient is thus very small.

We can see that the fit of approximate and exact seismograms is nearly perfect. This we could expect if we took into account the results shown in Figure 2. We can see very mild differences only at the traces immediately above the interface. The differences are caused by larger errors of the spreading in this region, see Figure 2.

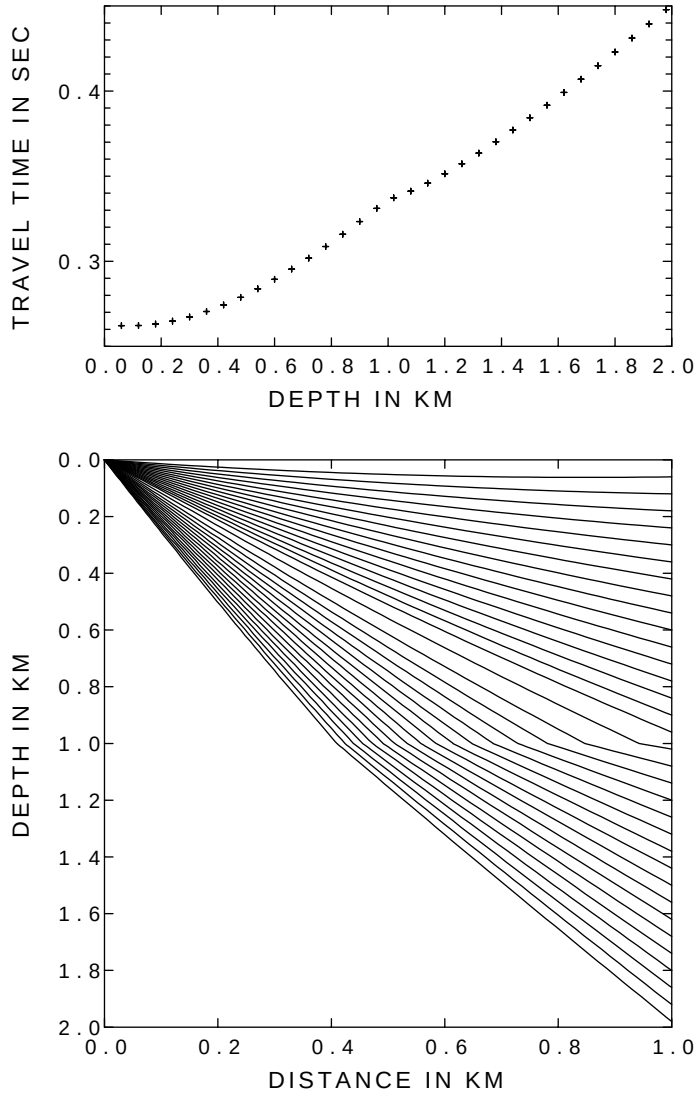

Figure 1: Ray diagram of the direct P wave, above the interface at the depth of 1 km and the transmitted P wave below the interface (bottom) in the "HTI/HTI" model. The corresponding traveltime curve (top).

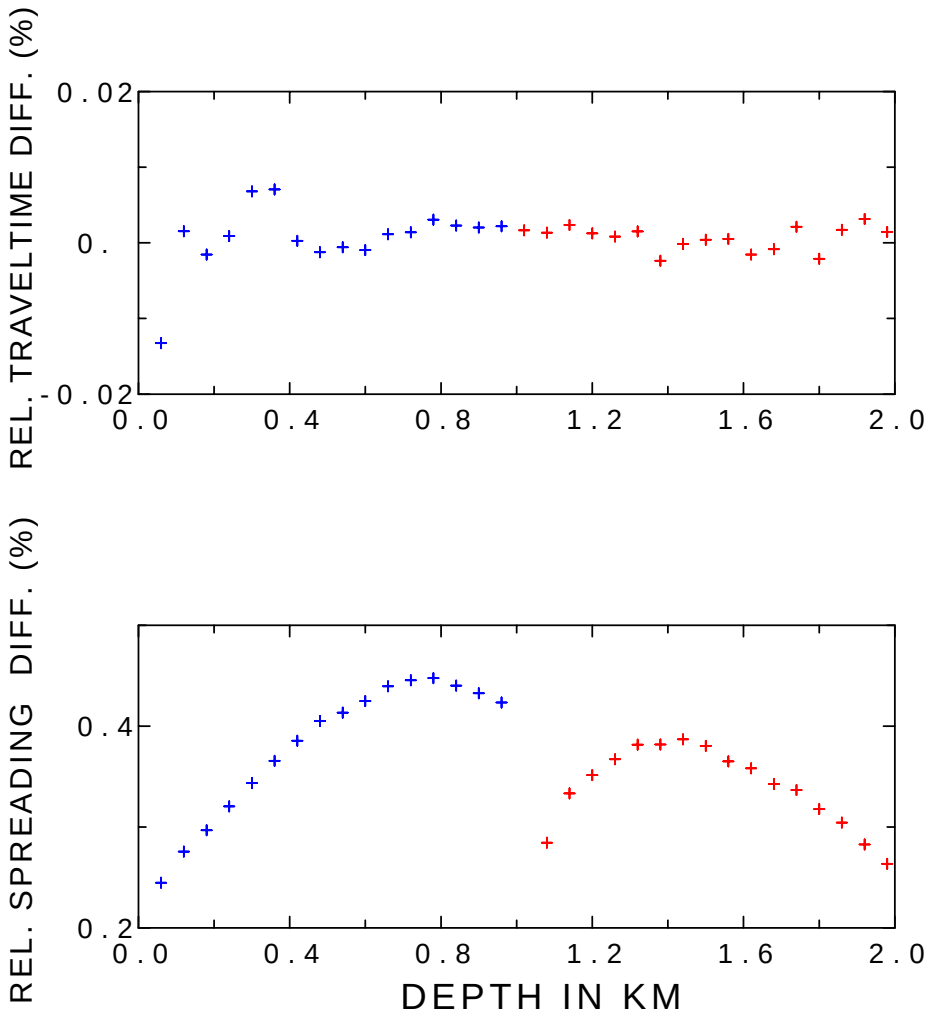

Figure 2: The relative second-order traveltime (top) and first-order spreading (bottom) errors for the reflected (blue) and transmitted (red) P wave in the "HTI/HTI" model. The interface is situated at 1 km depth.

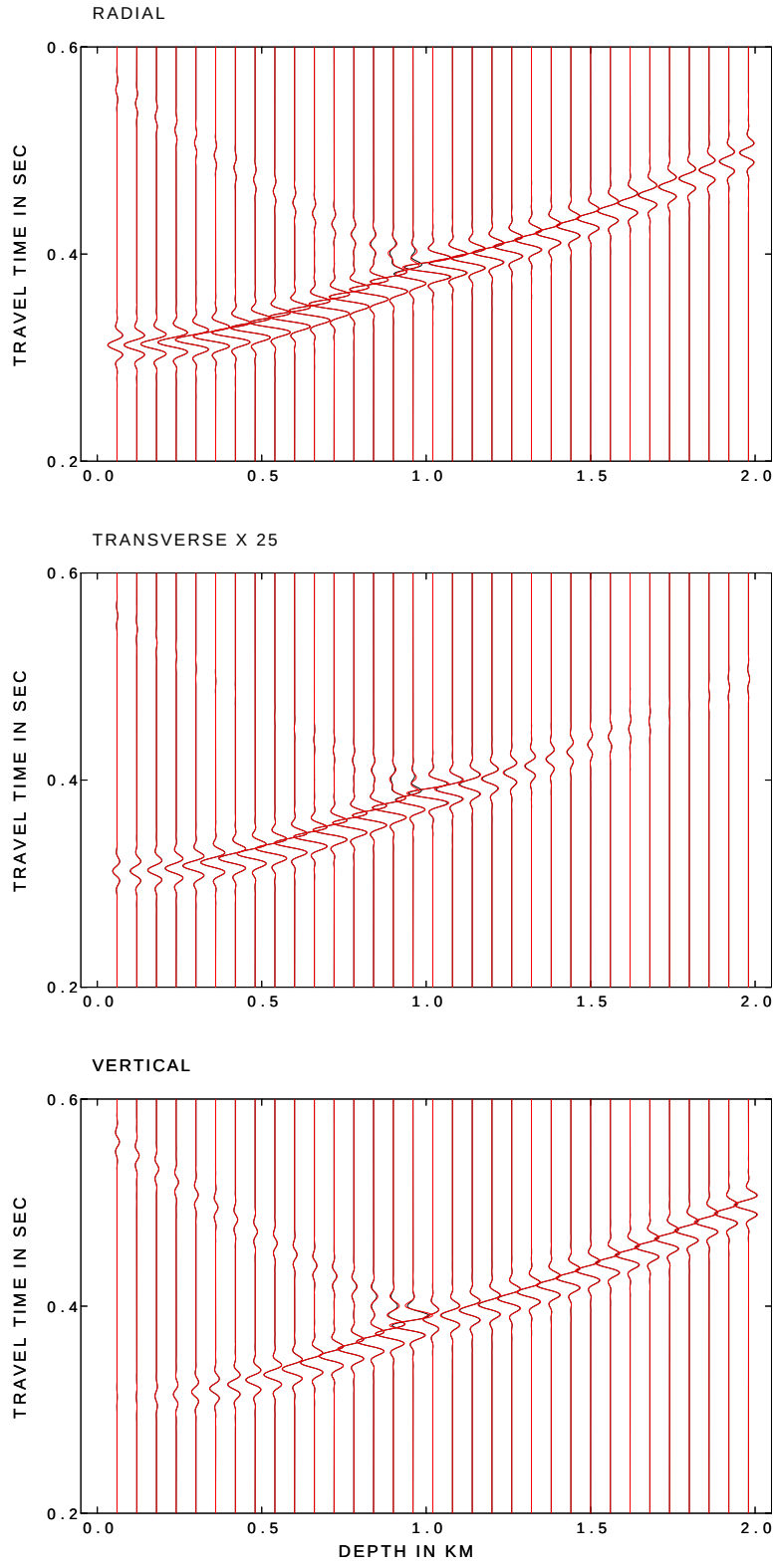

Figure 3: Comparison of exact (black) and first-order (red) P-wave ray synthetic seismograms of direct, reflected and transmitted waves generated by the vertical single-force source in the "HTI/HTI" model. Second-order traveltime correction (6) and (7) is used. Note the amplification of the transverse component.

7.2 ORT/ORT model

This model consists of the orthorhombic layer overlying the orthorhombic halfspace. Its anisotropy is around 20%. In the layer, the matrices of the density-normalized elastic moduli are:

$$\begin{pmatrix} 9.00 & 3.60 & 2.25 & 0.00 & 0.00 & 0.00 \\ & 9.84 & 2.40 & 0.00 & 0.00 & 0.00 \\ & & 5.94 & 0.00 & 0.00 & 0.00 \\ & & & 2.00 & 0.00 & 0.00 \\ & & & & 1.60 & 0.00 \\ & & & & & 2.18 \end{pmatrix} \tag{32}$$

at $z = 0$ km, and

$$\begin{pmatrix} 12.60 & 5.04 & 3.15 & 0.00 & 0.00 & 0.00 \\ & 14.11 & 3.36 & 0.00 & 0.00 & 0.00 \\ & & 8.32 & 0.00 & 0.00 & 0.00 \\ & & & 2.80 & 0.00 & 0.00 \\ & & & & 2.24 & 0.00 \\ & & & & & 3.05 \end{pmatrix} \tag{33}$$

at the interface depth, $z = 1$ km. The top matrix is used as shown, the bottom matrix is first rotated by 45^0 around z-axis, and then the z-axis is rotated by 45^0 around the new y-axis. Between $z = 0$ and $z = 1$ km, the parameters vary linearly with the depth. The halfspace is specified by the matrix with the density-normalized elastic moduli:

$$\begin{pmatrix} 19.80 & 7.92 & 4.95 & 0.00 & 0.00 & 0.00 \\ & 21.65 & 5.28 & 0.00 & 0.00 & 0.00 \\ & & 13.07 & 0.00 & 0.00 & 0.00 \\ & & & 4.40 & 0.00 & 0.00 \\ & & & & 3.52 & 0.00 \\ & & & & & 4.80 \end{pmatrix} . \tag{34}$$

At $z = 1$ km, the matrix (34) is first rotated by 45^0 around z-axis, and then the z-axis is rotated by 45^0 around the new y-axis. At $z = 3$ km, the matrix (34) remains unrotated. In between, as the depth varies, the parameters vary again linearly.

Figure 4 shows the relative errors of the second-order travel time (top) and of the first-order spreading (bottom). The blue crosses correspond again to the reflected wave (between depths 0 and 1 km) and the red crosses to the transmitted wave (between depths of 1 and 2 km). Despite considerably stronger anisotropy, traveltime errors remain less than 0.02% as in the "HTI/HTI" model. Chaotic behaviour of the relative travel time errors is again due to the two-point ray tracing procedure. The relative spreading errors are now considerably larger than in the "HTI/HTI" model. Maximum errors are close to 8%. The distribution of the errors of the reflected wave is very similar (but with the opposite sign) to that of the "HTI/HTI" model. The distribution of the errors of the transmitted wave is different. The largest errors can be observed immediately below the

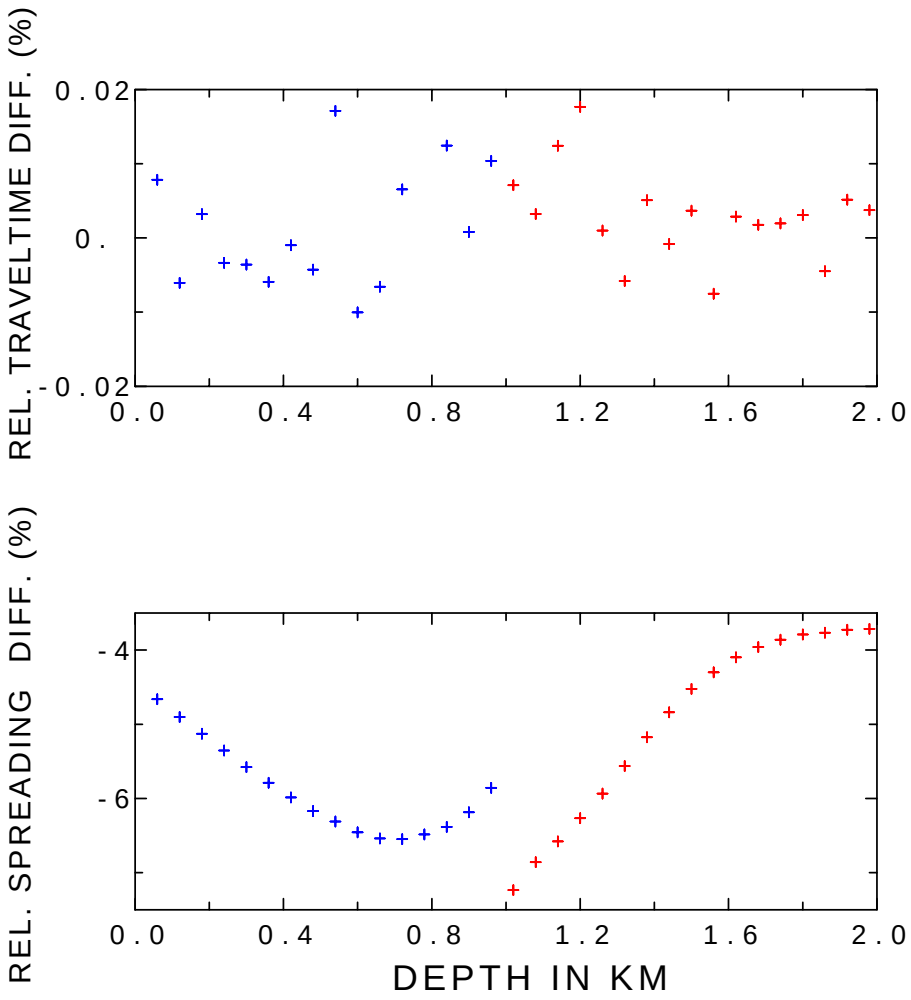

Figure 4: The relative second-order traveltime (top) and first-order spreading (bottom) errors for the reflected (blue) and transmitted (red) P wave in the "ORT/ORT" model. The interface is situated at 1 km depth.

interface. They decrease with increasing depth. Generally, the spreading errors are smaller than in a smooth medium (Pšenčík and Farra, 2007).

The corresponding ray synthetic seismograms are shown in Figure 5. We can see again the exact seismograms (black) overlayed by seismograms generated with the use of FORT and FODRT (red). Although anisotropy of the "ORT/ORT" model is considerably stronger, we can observe similar features, which we have already observed in Figure 3. First of all, there are negligible differences between approximate and exact seismograms. We can observe only some small differences at the shallowest receivers and then at receivers close to the interface, which are consequence of the errors in the spreading, see Figure 4. We can see strong direct and transmitted waves, but weak subcritical reflections. Transverse components are again very weak. Note that the transverse component is amplified 10 times with respect to the vertical and radial components. Since the source is situated in the symmetry plane (which rotates with increasing depth), the transverse components of direct and reflected waves are significantly smaller than those of the transmitted wave. The transmitted wave propagates off the symmetry plane and, therefore, it develops also weak, nevertheless more significant transverse component.

8 Conclusions

Presented tests indicate that accuracy of P-wave FORT computations remains quite high even for subcritically reflected and transmitted waves in layered media of weak to moderate anisotropy. As in the case of smooth media, accuracy of the spreading computations is lower than the accuracy of traveltimes (remember, second-order traveltimes were used in all computations). Despite of this, ray synthetic seismograms generated by FORT and FODRT fit exact seismograms perfectly even for anisotropy of about 20%.

The next steps in our study will be extension of the above-presented results to the critical and overcritical regions and incorporation into the computations of converted waves, generated by the incidence of a P wave at an interface.

Acknowledgements

A substantial part of this work was done during IP's stay at the IPG Paris at the invitation of the IPGP. We are grateful to project "Seismic waves in complex 3-D structures" (SW3D) and Research Project 210/11/0117 of the Grant Agency of the Czech Republic for support.

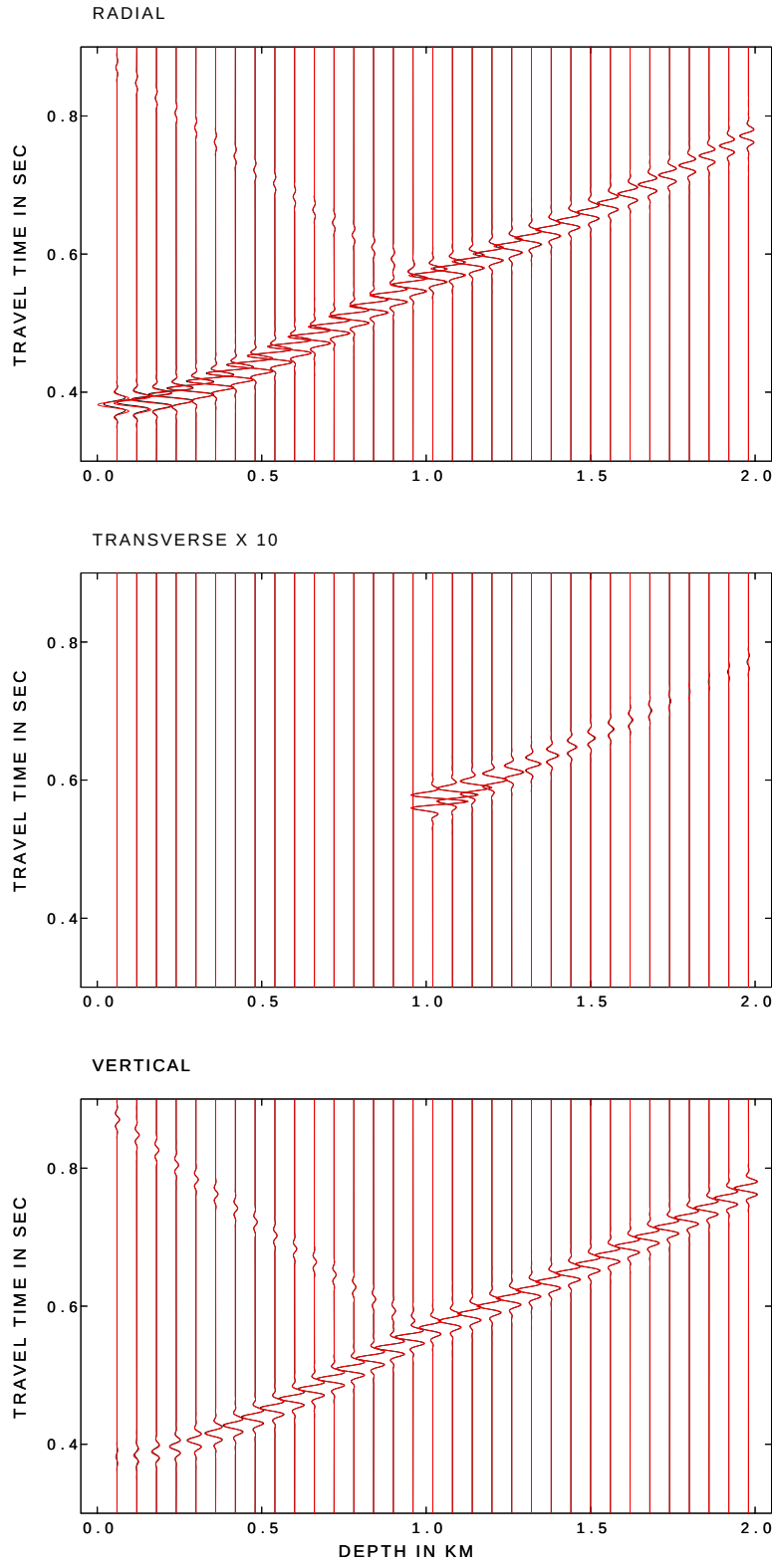

Figure 5: Comparison of exact (black) and first-order (red) P-wave ray synthetic seismograms of direct, reflected and transmitted waves generated by the vertical single-force source in the "ORT/ORT" model. Second-order traveltime correction (6) and (7) is used. Note the amplification of the transverse component.

REFERENCES

Červený, V., 2001. *Seismic Ray Theory*, Cambridge Univ. Press, Cambridge.

Dehghan, K., Farra, V. and Nicolétis, L., 2007. Approximate ray tracing for qP-waves in inhomogeneous layered media with weak structural anisotropy. *Geophysics*, **72**, SM47–SM60.

Farra, V., and Le Bégat, 1995. Sensitivity of qP-wave traveltimes and polarization vectors to heterogeneity, anisotropy and interfaces. *Geophys. J. Int.*, **121**, 371–384.

Farra,V. and Pšenčík,I., 2010. First-order reflection/transmission coefficients for unconverted plane P waves in weakly anisotropic media. *Geophys.J.Int.*, **183**, 1443–1454.

Gajewski,D., and Pšenčík,I., 1987. Computation of high-frequency seismic wavefileds in 3-D laterally inhomogeneous anisotropic media. *Geophys.J.R.astr.Soc.*, **91**, 383–411.

Gajewski, D., and Pšenčík, I., 1990. Vertical seismic profile synthetics by dynamic ray tracing in laterally varying layered anisotropic structures, *J. Geophys. Res.*, **95**, 11301–11315.

Pšenčík, I., and Farra, V., 2005. First-order ray tracing for qP waves in inhomogeneous weakly anisotropic media. *Geophysics*, **70**, D65–D75.

Pšenčík,I. and Farra,V., 2007. First-order P-wave ray synthetic seismograms in inhomogeneous weakly anisotropic media. *Geophys.J.Int.*, **170**, 1243–1252.